

Research Article

Low-Cost Multisensor Integrated System for Online Walking Gait Detection

Lingyun Yan ¹, Guowu Wei ², Zheqi Hu,¹ Haohua Xiu,³ Yuyang Wei,¹ and Lei Ren ¹

¹*School of Mechanical, Aerospace and Civil Engineering, The University of Manchester, Manchester, M13 9PL, UK*

²*School of Science, Engineering and Environment, University of Salford, Salford M5 4WT, UK*

³*College of Biological and Agricultural Engineering, Jilin University, Changchun, Jilin 130000, China*

Correspondence should be addressed to Guowu Wei; g.wei@salford.ac.uk and Lei Ren; lei.ren@manchester.ac.uk

Received 21 April 2021; Revised 2 July 2021; Accepted 25 July 2021; Published 14 August 2021

Academic Editor: Carlos Ruiz

Copyright © 2021 Lingyun Yan et al. This is an open access article distributed under the Creative Commons Attribution License, which permits unrestricted use, distribution, and reproduction in any medium, provided the original work is properly cited.

A three-dimensional motion capture system is a useful tool for analysing gait patterns during walking or exercising, and it is frequently applied in biomechanical studies. However, most of them are expensive. This study designs a low-cost gait detection system with high accuracy and reliability that is an alternative method/equipment in the gait detection field to the most widely used commercial system, the virtual user concept (Vicon) system. The proposed system integrates mass-produced low-cost sensors/chips in a compact size to collect kinematic data. Furthermore, an x86 mini personal computer (PC) running at 100 Hz classifies motion data in real-time. To guarantee gait detection accuracy, the embedded gait detection algorithm adopts a multilayer perceptron (MLP) model and a rule-based calibration filter to classify kinematic data into five distinct gait events: heel-strike, foot-flat, heel-off, toe-off, and initial-swing. To evaluate performance, volunteers are requested to walk on the treadmill at a regular walking speed of 4.2 km/h while kinematic data are recorded by a low-cost system and a Vicon system simultaneously. The gait detection accuracy and relative time error are estimated by comparing the classified gait events in the study with the Vicon system as a reference. The results show that the proposed system obtains a high accuracy of 99.66% with a smaller time error (32 ms), demonstrating that it performs similarly to the Vicon system in the gait detection field.

1. Introduction

Since its development in the 1970s, modern gait identification and analysis has been widely used in walking rehabilitation, gait training, life assistance, and motion monitoring [1–4]. In addition, the gait detection system is widely applied in the exoskeleton since it is capable of identifying walking patterns [5, 6].

Three-dimensional motion analysis (3DMA) is the gold standard for biomechanical analysis since it records the most accurate kinematic data [7]. However, the typical motion capture system (Vicon system) is expensive and difficult for marker application and has slow data postprocessing. The camera-based two-dimension analysis is an alternative method to detect movement and is proven to work effectively in gait analysis in various environments [8]. However, its

accuracy is limited due to the lack of one dimension in 3D coordinates. Besides, the image signal is prone to observer bias and leads to unreliability [7, 8]. On the other hand, video recording generated a vast amount of data and required a high computing performance [9]. These drawbacks limited the use of two-dimensional visual analysis in gait analysis.

Wearable sensors work effectively in recording kinematic data, whereas various gait detectors have been developed under the combination of low-cost sensors. These gait detectors include manual switches [10, 11], foot switches [10, 11], shank inclinations [12], force-sensitive resistors [13], goniometers [14, 15], gyroscopes [16], accelerometers, and electromyography (EMG) sensors [17–20]. These sensors could be used to detect the walking pattern and identify the gait phases. However, most of these sensors are mounted

separately around the body which makes them difficult for wearing or experimenting with. Instrumented shoes/insole with different sensor technologies were created in response to a demand for a portable kinematic data collection system.

The instrumented shoes/insoles were widely developed by different research groups that combined various sensors for kinematic data collection, and this contributed to their widespread acceptance [21]. Force sensors, gyroscopes, and accelerometers are widely used for gait detection or emulating patients' diseases such as foot illness, structural disorders, and early diagnosed pathologies [22]. These plantar pressure analysis shoes could estimate the mean pressure, peak pressure, and central pressure of the foot, as well as balance analysis, ground reaction force detection, and spatiotemporal gait assessment. Furthermore, these wearable sensors showed a promising result in gait phase detection on both healthy and pathological populations [23–31]. Therefore, adopting a highly integrated digital insole design is a good plan for the exoskeleton design to balance wearing ease and gait detection accuracy.

A proper online gait event detection (GED) algorithm must deal with the inertial signals and ground reaction forces. Some existing online algorithms have been presented on the basis of inertial signals [32–36]. The signal of the gyroscope could be used to determine the initial contact and toe-off stages, whereas the acceleration is used to detect the foot-flat and toe-off [34]. Most of these threshold filter-based gait detection systems showed some similarity with a rule-based gait phase detection system (GPDS) which was put forward by Pappas et al. [37]. The GPDS divides a gait cycle into four stages: heel-strike, stance, heel-off, and swing. Furthermore, the switch of four gait phases was classified by the filter-based algorithm. Also, this simple rule-based gait detection algorithm could achieve considerable performance compared to the hidden Markov model (HMM) approach [36].

However, most of them adopt threshold filters, which create computational burden and delays due to the complex mathematical calculation required for threshold value updates [33, 34]. In addition, machine learning (ML) showed superior performance in boundary decision and classification [38]. When large training data was fed, the ML-stetted boundaries produced better decision accuracy than the manual threshold [39]. Some ML methods like neural networks (NNET) and support vector machines have been applied in automatic gait recognition [40–42]. The artificial NNET was designed using features extracted from walking kinematic parameters.

This study is aimed at designing a reliable low-cost online GEDS performance and comparing it to a commercial system. To lower the cost, the proposed system adopts mass-product sensors and chips, while an x86 mini-PC was used as a computing center to run the gait detection algorithm in real time. To guarantee the gait detection accuracy, the proposed system adopts a four-layer MLP model and a rule-based calibration filter to classify kinematic data into five distinctive gait events: heel-strike, foot-flat, heel-off, toe-off, and initial-swing.

Another aim is to compare the performance of the two systems; therefore, walking experiments are being planned

to determine if the low-cost system can replace the commercial system. The result indicates that the proposed system achieves high performance of 99.66% accuracy with employed feature extraction, hyperparameter optimisation, and rule-based calibration. With regard to the fast-computing demand, a short sliding time window (10 ms) and a simple MLP structure are used as they have the characteristics of less processing and response time. These intrinsic characteristics lead to a smaller time error (32 ms) compared to other gait detection systems [32–34, 43, 44]. Finally, these findings prove that the low-cost system has a similar performance to the commercial system and reaches the design target.

2. Physical Model

A control board and two digital insoles make up the low-cost multisensor integrated system (LMIS). Figure 1 shows that the integrated structure is lightweight and portable. The digital insole collects the foot's kinematic data during walking, while the control board classifies the data into five gait events through an embedded gait detection algorithm.

2.1. Digital Insole. The digital insole is assembled by a UK 8 size insole, two square FSR (Interlink Electronics FSRTM 400 series), and a 9-axis IMU (MPU 9250) as shown in Figure 1(c). The orientation of IMU is calculated by the Kalman filter which was widely applied to unmanned aerial vehicles [45]. The acceleration and angular measurement ranges of MPU-9250 are ± 16 g and ± 2000 deg/s, respectively, and for each measurement, the precision is 6×10^{-5} g and 8×10^{-3} deg/s. The force accuracy range of square FSR is $\pm 5\%$ to $\pm 25\%$. One FSR is located in front of the insole to detect the toe load while the other is located at the back for the heel load measurement. Meanwhile, the IMU is mounted under the foot arch, which is the best place around the foot for placing a sensor as it delivers the most accurate data [46]. Also, in this location, the chip sustains the smallest foot pressure and prevents damage.

2.2. Control Board. Figure 1 shows that the physical structure of the control board is a cuboid box (310 mm \times 110 mm \times 150 mm), which is lightweight and portable. It consists of two Arduino Uno R3, an x86 mini-PC, and a power bank. Furthermore, the control system is divided into two levels: a low-level controller and a high-level controller.

Uno R3 is the core of a low-level controller which is embedded in a 16 MHz microcontroller, and it is mounted on a breadboard and connected to the digital insole's cable. The applied force on the insole can be calculated by measuring the voltage as the resistance of FSR would change according to varied pressure. Furthermore, the raw acceleration/gyration data in IMU are sent to Uno R3 by the I2C port. The Uno R3 acquires the kinematic data of the digital insole, then the output to the mini-PC.

The x86 mini-PC is a high-level controller that has high computing performance as it is powered by a 1.1 GHz Intel M3-8100Y chip. A 10000 mAh power bank supplies electricity to both the Uno R3 and the mini-PC. The mini-PC receives preprocessed kinematic data from the low-level

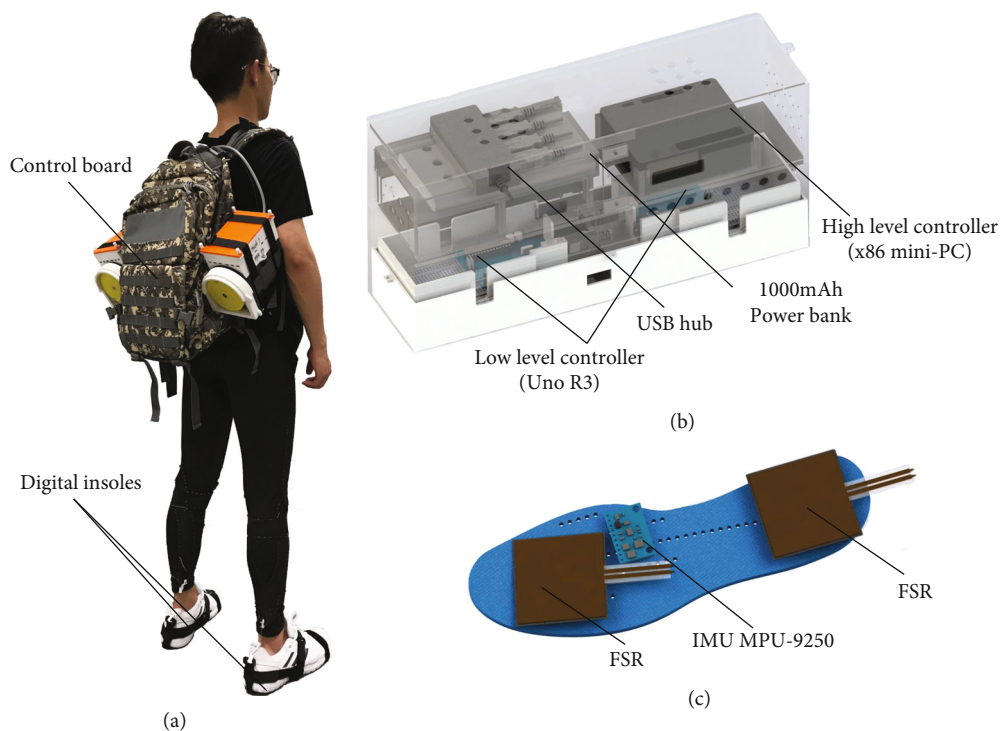


FIGURE 1: Low-cost multisensor integrated system: (a) subject with LMIS; (b) assembled control board; (c) disassembled digital insole.

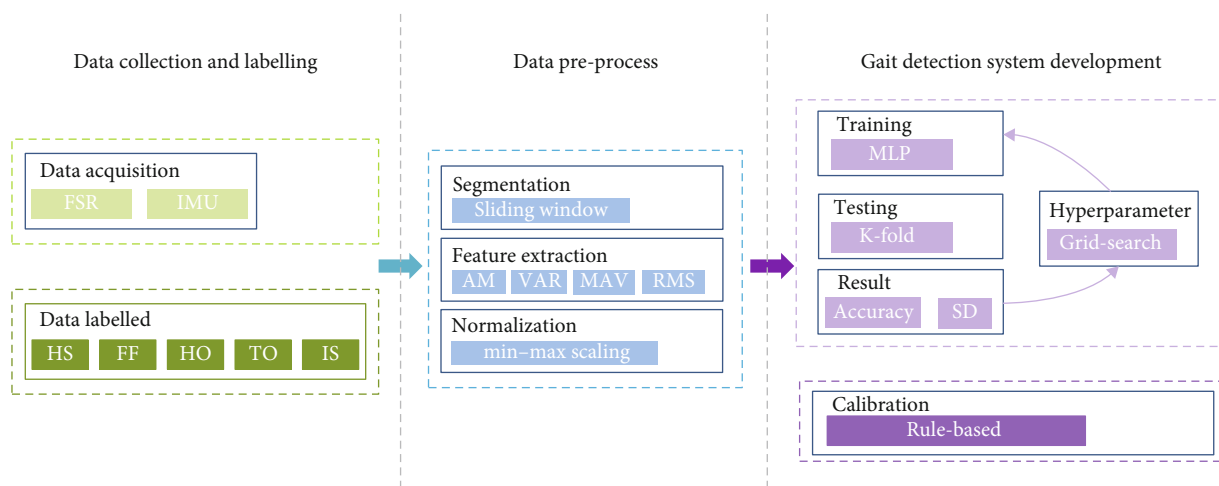


FIGURE 2: Development process of LMIS.

controller and classifies the gait event in real time by the ML-based gait detection algorithm. For data transmission, the IMU sends data to the Uno R3 through the I2C Protocol, and Uno R3 sends kinematic data to the x86 mini-PC by a serial port through a USB.

3. Gait Detection Algorithm Modeling

Figure 2 shows the development of the gait detection algorithm of LMIS based on ML and the rule-based calibration method. This algorithm is designed to detect the five gait

events: heel-strike(HS), foot-flat (FF), heel-off (HO), toe-off (TO), and initial-swing (IS) in real time at 100 Hz. Keras package is selected to run the GED algorithm on the Python® platform. Besides, MLP was adopted to establish the NNET in this paper as it shows good performance in solving stochastic problems and can establish a mapping from complex input data to outputs. The MLP predicts the real-time gait event based on the signals of IMU embedded in the insole when FSR data are adopted for rule-based calibration. This rule-based calibration filter is applied to cross-validate the gait prediction from the MLP model.

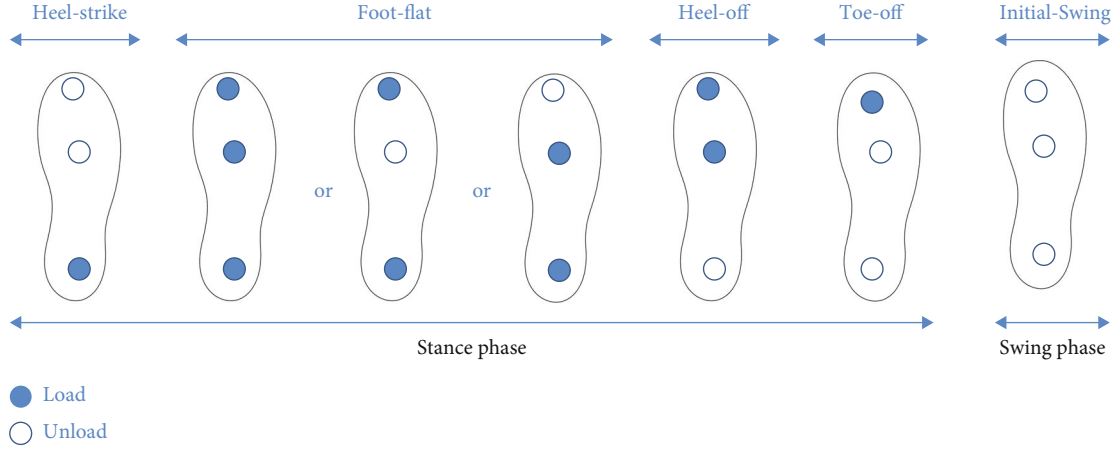


FIGURE 3: Gait event labelling criteria according to 3-FSR measurement.

3.1. Gait Event and Labelling Method. The gait event is divided into the stance phase and the swing phase. Therefore, for better analysis of walking patterns, the gait event is subdivided into the following five events: HS, FF, HO, TO, and IS.

MLP should be trained first before employing the low-cost gait detection system. The training dataset generated by IMU in the digital insole is labelled by additional measurement equipment. In this research, three rounded FSRs (SPARKFUN SEN-09375) were attached to the shoe button to measure the foot pressure. One was mounted on the shoe upper front, one located on the toe area, and the last fixed on the heel area. Also, the FSR connected with Uno R3, so the kinematic data acquisition and data labelling process could work simultaneously.

Figure 3 shows the method to determine individual gait events according to the 3-FSR measurement result. A 10N threshold decides the load/unload condition; the FSR load larger than the threshold is defined as a load condition and vice versa. Finally, the gait event is labelled according to the load conditions. The force larger than 10N applied on FSR is defined as the load condition and any smaller force applied is the unloaded condition.

3.2. Data Acquisition. The collection of foot kinematic data by the insole and 3-FSR are running simultaneously with Uno R3 at 300Hz. The 3-FSR only obtains 3 load values when each insole's dataset contains 8 parameters that are 3-axis accelerations, 3-axis angular velocities, and 2 load values. Besides, the MLP model makes use of the 6-axis IMU data when 2 load forces are applied for rule-based calibration. An integrated message of each insole is composed of a timestamp, IMU data, FSR data, and labels, in that order.

3.3. Feature Extraction and Data Preprocessing. This study mainly focuses on time-domain feature extractions as the sampling frequency of the Uno R3 board is too low for Fourier transform. The features of IMU signals are extracted for MLP training and classification. Four time-domain features have been extracted in this project: arithmetic mean (AM), mean absolute value, root mean square, and variance (VAR). In

equation (1), x_i represents the input values and N stands for the number of inputs.

$$\left\{ \begin{array}{l} \text{AM} = \frac{1}{N} \sum_{i=1}^N x_i, \\ \text{MAV} = \frac{1}{N} \sum_{i=1}^N |x_i|, \\ \text{RMS} = \sqrt{\frac{1}{N} \sum_{i=1}^N x_i^2}, \\ \text{VAR} = \frac{1}{N-1} \sum_{i=1}^N x_i^2. \end{array} \right. \quad (1)$$

This research applies a 10 ms sliding window to extract data features, as a complete gait cycle only takes around 0.6 s and requires a short response time. By this method, the raw data could be extracted into one-dimension vectors (24 parameters) at 100 Hz.

Since the extracted features have different scales, the significant difference could cause classification problems when these different values are adopted together for ANN training. To solve this problem, a min-max scaling normalisation is adopted to rescale the range of features to the common range in $[-1, 1]$.

$$x' = a + \frac{(x - \min(x))(b - a)}{\max(x) - \min(x)}. \quad (2)$$

In this formula, the a and b represent the rescaled range $[a, b]$. In this paper, a is -1 and b equals 1. x represents the feature values when $\min/\max(x)$ stands for the minimum and maximum values in the dataset. After that, the normalised one-dimension vectors are the output for the MLP model.

3.4. MLP Modelling and Evaluation. A baseline MLP model is established to classify the gait event based on the data type of

input/output. It has 24 input nodes and 5 output nodes because of the 24 gait parameter inputs and 5 gait event outputs. Therefore, it introduces a k -fold cross-validation method to test the model performance. The k -fold cross-validation procedure divides a limited dataset into k non-overlapping folds. Each k -fold has a chance to be used as a held-back test set when all other folds are used as a training dataset. A total of k models is fit and evaluated, and the mean performance is reported. In formula (3), CV represents the mean performance, indicating the iteration of models whereas k is the number of folds.

$$CV = \frac{1}{k} \sum_{i=1}^k \text{accuracy} (i). \quad (3)$$

By adopting a k -fold evaluation, the AM over the k performance estimates from the test sets could be calculated. Also, it reduces the pessimistic bias significantly compared to a single-fold accuracy calculation.

3.5. Hyperparameter Optimisation. The ANN model has a complex structure with different constraints, weights, batch size, learning rate, and neurons to generalise different data patterns. Hyperparameter optimisation searches for the most optimal combination of ANN parameters to achieve the best performance. In this research, the grid search is applied in the MLP model and it searches for the most optimal neuron numbers and batch size. Besides, the fivefold cross-validation was applied to evaluate the performance.

According to the grid search result in Figure 4(a), the optimal hyperparameters of the MLP model could reach 96.25% accuracy with a small standard deviation (0.0202) when this model adopts 6 neurons in layer 1, 2 neurons in layer 2, and batch size sets to 8.

3.6. Rule-Based Calibration Filter. The MLP model achieves 96.25% gait detection accuracy after hyperparameter optimisation. However, this accuracy is not enough for the exoskeleton control, as the incorrect assistive force leads to uncoordinated walking. Figure 5 shows a rule-based filter being introduced to calibrate the MLP results and improve gait detection accuracy. It calibrates the gait event prediction of MLP by some threshold condition judgments.

Based on the training dataset, we found some common errors occurring in the neural network. ANN tends to confuse some FF with HS phases as, in the first place, FF has a similar IMU pattern with the HS phase. However, the HS can only happen sequentially after the IS and cannot appear in the middle of any stance phase. So, this introduces the “previous gait” to store the previous gait phase. Once the previous gait event of HS is not IS, algorithms should deny the prediction and continue using the last gait phase until they get a new prediction. Also, in the heel-strike event, the toe load should be smaller than 100 N as the toe area has not had contact with the ground yet.

When it comes to foot-flat, both the heel and toe loads stay at a high level because the foot fully contacts the ground. Also, the value of the force applied on two FSRs are much higher than 100 N in all subject experiment data. And the

100 N is taken as the threshold to determine whether the toe/heel contacts the ground. If the heel load intends to decrease and the toe load remains at a high-pressure level, it means that the subject comes to the heel-off stage. Furthermore, the toe-off event only occurs after the stance or heel-off, and this circumstance can be used to correct the wrong MLP prediction. Meanwhile, only a small amount of force was applied to the two FSRs during the IS. In this case, both FSRs sustain smaller load values compared to the threshold. Once the artificial NNET is combined with the rule-based filter, the gait detection algorithm achieves high accuracy and reliability.

4. Experiments

4.1. Experiment Scenarios. The experiment acquires the gait event of subjects during walking by two different systems. The first is the custom LMISL developed in the Python platform, whereas the second is the commercial Vicon system. The paper is aimed at comparing the GED result between the low-cost system and commercial systems to evaluate the accuracy and reliability of the custom systems. Thus, five subjects were required to walk on a treadmill at a normal walking speed (4.2 km/h) under two systems for data collection and gait event classification. Figure 6 shows the experimental arrangement of the two systems.

In the data acquisition process of the gait detection experiment, five able-bodied subjects voluntarily participated and their information are listed (see Appendix Table A1). The subjects were informed of the purpose and procedures of the study, and a written consent form was signed by each subject. The experimental design was approved by the Ethics Committee of the Second Hospital of Jilin University, and the study was conducted according to the Declaration of Helsinki.

For customer low-cost systems, the digital insoles are put inside the shoes for data collection. Then, the IMU/FSR sends the raw electric signal to the Arduino board for processing and conversion to kinematic data. Afterward, the kinematic data delivered to the mini-PC are classified into gait events by NNET.

Furthermore, the commercial Vicon system is an infrared motion capture system that tracks the position of reflective markers in 3D space. Figure 6, (2), shows four reflective balls attached to the subject’s shoe before the experiment. The vintage camera captures the marker’s reflected light and determines the 2D coordinates of the markers, whereas the 3D coordinates would be composed of six 2D coordinates from six cameras. The coordinate information is recorded in the host PC and postprocessed for gait event classification.

Figure 7 shows the experimental procedures of two systems running independently to detect the gait event, and the gait result of the Vicon system is taken as the reference. Since two systems work independently, it is necessary to synergise the two systems into the same timeline before the calculation of accuracy. The timeline synergy method is mainly based on recording the time of the first gait event in both systems set as the base time, as indicated in Figure 8. At the start of the experiment, the subjects were requested

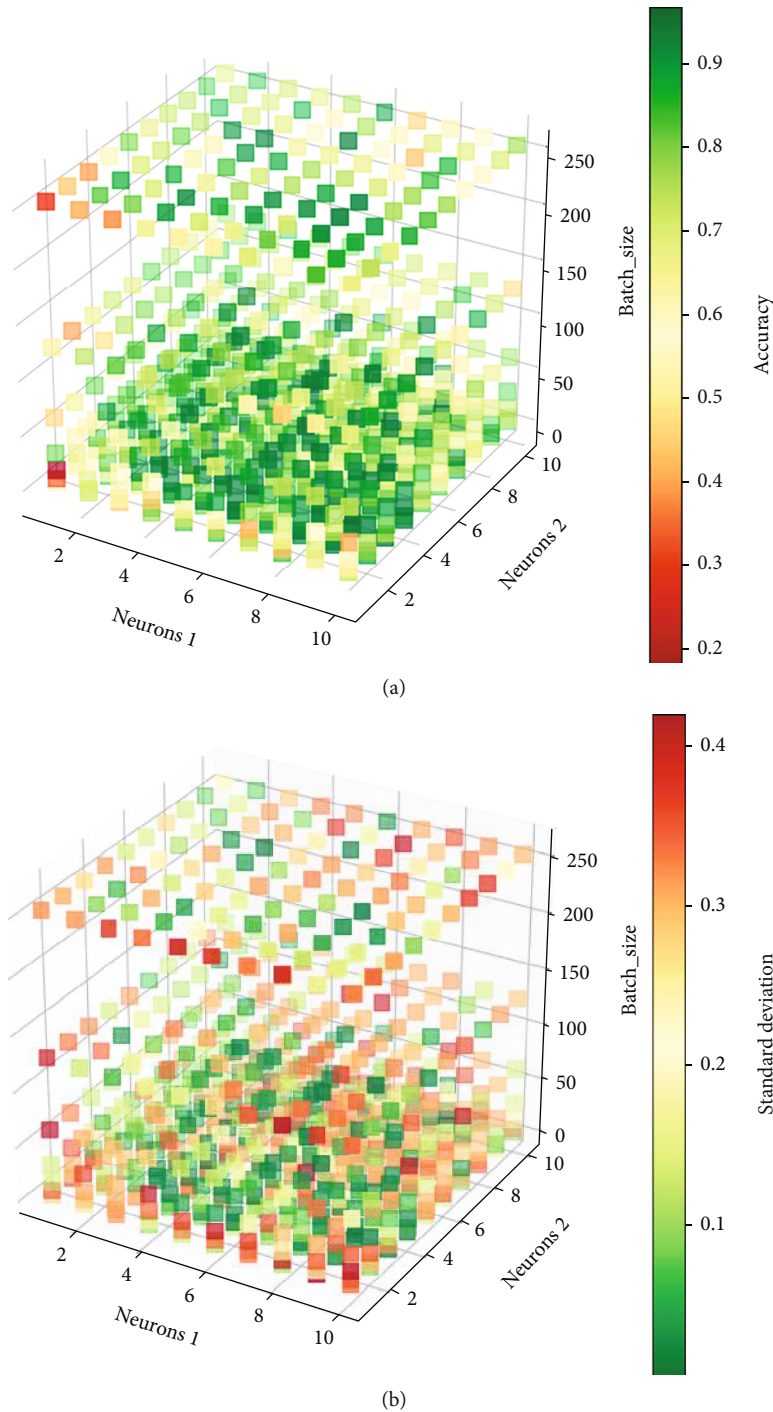


FIGURE 4: Hyperparameter optimisation: (a) accuracy of grid search result; (b) standard deviation of grid search result.

to stand near the force plate and lift their feet off the ground at 10 s, then step on the force plate and walk on the treadmill. The time the force plate and the digital insole was loaded was identified as the time axis zero point in both systems.

After that, two systems worked simultaneously to record the walking pattern until the stop of the treadmill. Then, all the experimental data were saved and synergised into the same timeline. Furthermore, the gait event results in both systems were determined and recorded into the same time-

line. At last, the accuracy and time error of a low-cost system could be evaluated by comparing the results with the reference.

4.2. Equipment

4.2.1. *Low-Cost System.* The low-cost system shown in Figure 6 is made up of 2 components: the control board and the digital insole. The physical components contain a

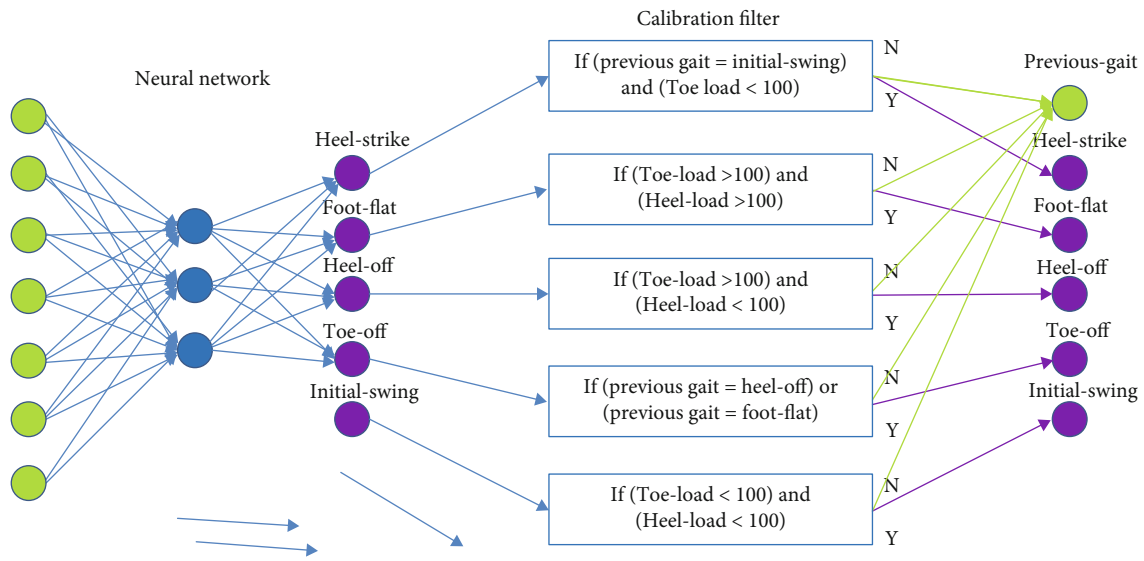


FIGURE 5: Gait detection algorithm diagram.

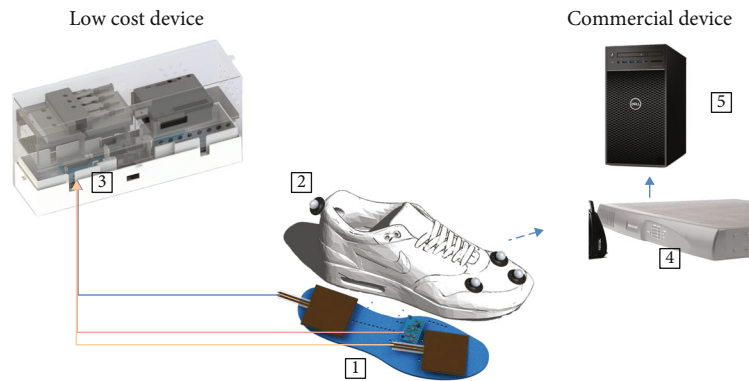


FIGURE 6: Equipment of the testbed used in the experiments: (1) digital insole (IMU and FSR embed); (2) Pearl Hard Base Markers; (3) control board (Uno R3, mini-PC, and power bank); (4) Vicon Vantage camera and Vicon lock unit; (5) host PC.

Latte panda mini-PC, Arduino board, power bank, IMU, and FSR. The sampling frequency of sensors is 300 Hz with the data features extracted by a 10 ms window and classified into gait events by the gait detection algorithm at 100 Hz.

The IMU and FSR are embedded in the digital insole and send the raw signal to the Arduino board. Besides, the Arduino board registers the information and delivers it to the mini-PC, where kinematic data are analysed and classified into gait events. A 10000 mAh power bank supplies electricity since the whole system is low energy cost. The main characteristic of the low-cost system is listed (see Appendix Table A2).

4.2.2. Commercial System. The second system used in the experiment is a commercial one (Vicon system) with characteristics as in Table 1. This equipment is widely used in motion capture and gait analysis because of its high accuracy and powerful platform. In this experiment, the working area of the Vicon system is 5 m × 5 m. The Vicon system consists of six V5 cameras and two force plates which run on the

Nexus TM software. The multiset of cameras could capture the motion at 200 Hz and the force plate at 1000 Hz.

In contrast with the low-cost system, this facility has a higher sampling frequency (up to 420 Hz) and no extra load on the subject since the equipment is fixed in the laboratory. The users are only required to stick with markers for IR camera tracking. However, offline postprocessing is required to classify the foot coordination data into gait events. The main characteristic of the Vicon system is listed (see Appendix Table A3).

4.3. Data Analysis. After the experiment, the kinematic data from the low-cost system and Vicon system should be analysed for gait event estimation. And the gait results of the two systems should be synergised into the same timeline before comparison and performance evaluation.

4.3.1. Low-Cost System. The gait detection algorithm predicts the gait event and records the kinematic data in real time, and the results are shown in Figure 9. The four subplots illustrate the gait events, foot load, acceleration, and foot angles,

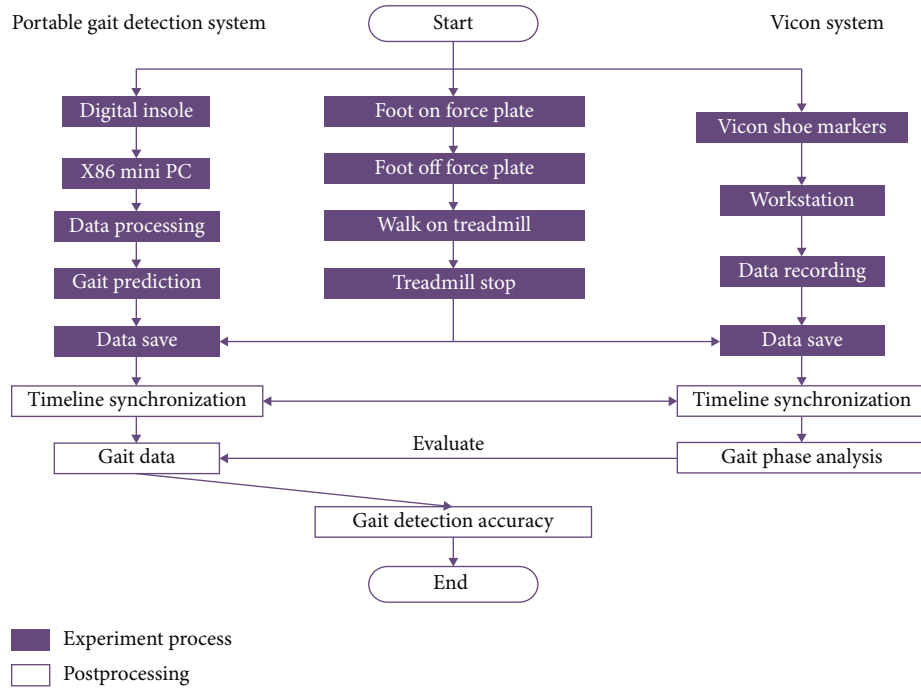


FIGURE 7: Experiment diagram.

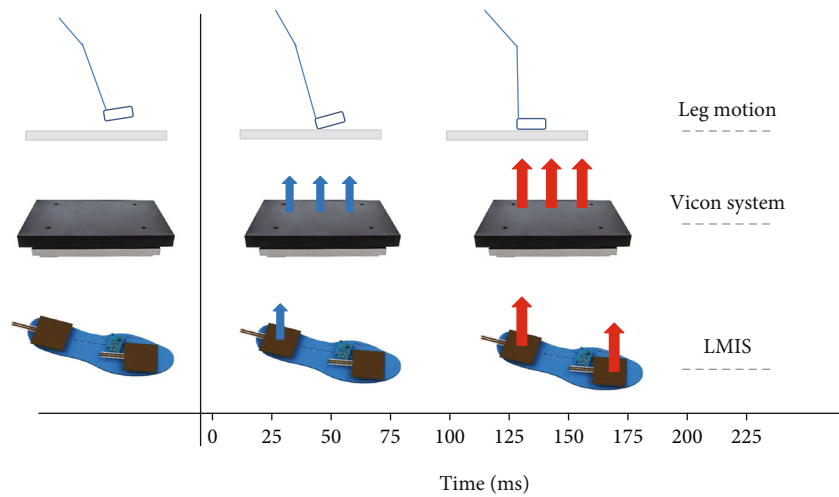


FIGURE 8: Timeline synergy method.

TABLE 1: Time error comparison among different gait detection systems.

Project	Heel-strike	Foot-flat	Time error (ms)			Initial-swing
			Heel-off	Toe-off		
LMIS	29	17	53	33	29	
GPDS [37]	70	70	40		35	
Skelly [43]	120	233	150	33	67	
González [32]	157.2			37.4		
Zhou [33]	146.6			70.4		
iIMU [44]	10			19		
Maqbool [35]	16	16.5	3.6	16		

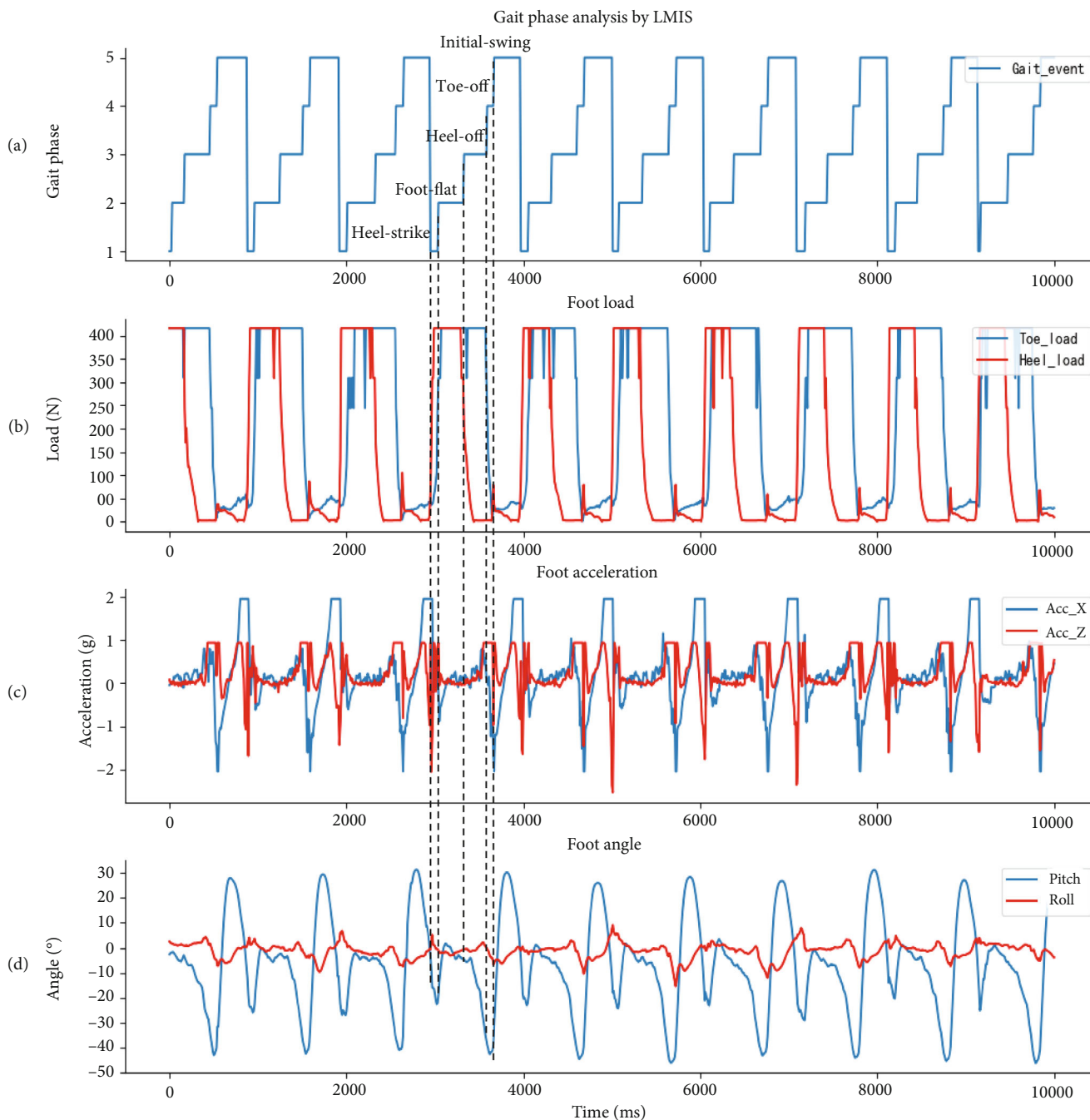


FIGURE 9: Gait phase detection by digital insole: (a) gait phase; (b) foot load; (c) foot acceleration; (d) foot angle.

respectively. Some common features can be extracted in a complete gait cycle since different kinematic parameters have similar periodicity. For example, surged heel load and plunged z-axis acceleration values always appeared at HS events. Similarly, in the TO stage, the value of the toe load and x-axis acceleration plunged at the same time. In FF, the z-axis acceleration stays around 0g, and the foot load stays at the highest level. When it comes to HO, both the foot pitch and heel load plunged. At the initial-swing event, the x-axis acceleration values get to the bottom and the foot load approached zero.

4.3.2. *Vicon System.* As the Vicon system records the 3D coordinates of four markers, it is easy to track foot movement and estimate the corresponding gait events. The three subplots illustrate the gait events, the z-axis coordinates the shoe marks, and the 3 axes coordinate the heel marker, respectively. Figure 10(c) indicates that the z-axis value of the heel marker descends to the bottom at every heel-strike event. Moreover, all marker values in the z-axis stay similar between the FF event and the HO event. The values of the heel marker surge when it comes to the HO stage as the foot goes off the ground. Once the value of the toe marker rises, it indicates

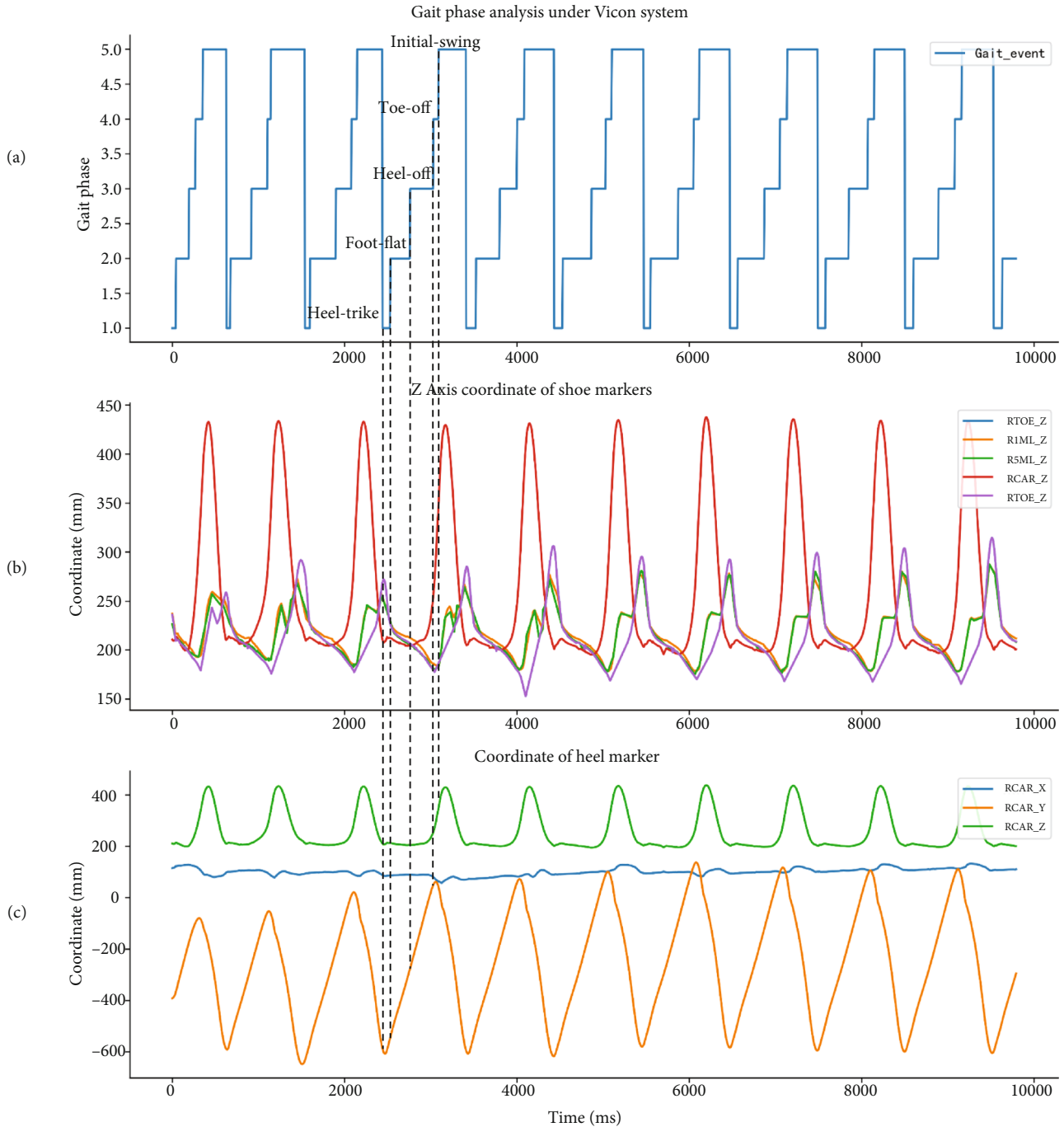


FIGURE 10: Gait event analysed by Vicon experiment data: (a) gait phase; (b) Z-axis coordination; (d) heel-marker coordination.

that the gait phase comes to TO. The period between the TO and the next heel HS is the swing phase.

4.3.3. *Gait Event Comparison.* Figure 11 shows the result of the two systems after determining the gait event of the walking experiment. The result indicates that the low-cost system achieves similar performance compared to the commercial system. However, Figure 11(c) shows the existence of some time error between the two systems. It is caused by different sampling frequencies and classification methods.

The performance of the low-cost system is evaluated in the result chapter.

5. Results and Discussions

5.1. *Gait Detection Accuracy.* The gait detection accuracy was evaluated by comparing the detected gait event from LMIS with Vicon’s result. The studied gait phase is considered to be the reference walking pattern since Vicon recorded the most accurate foot coordinate value at a high frequency.

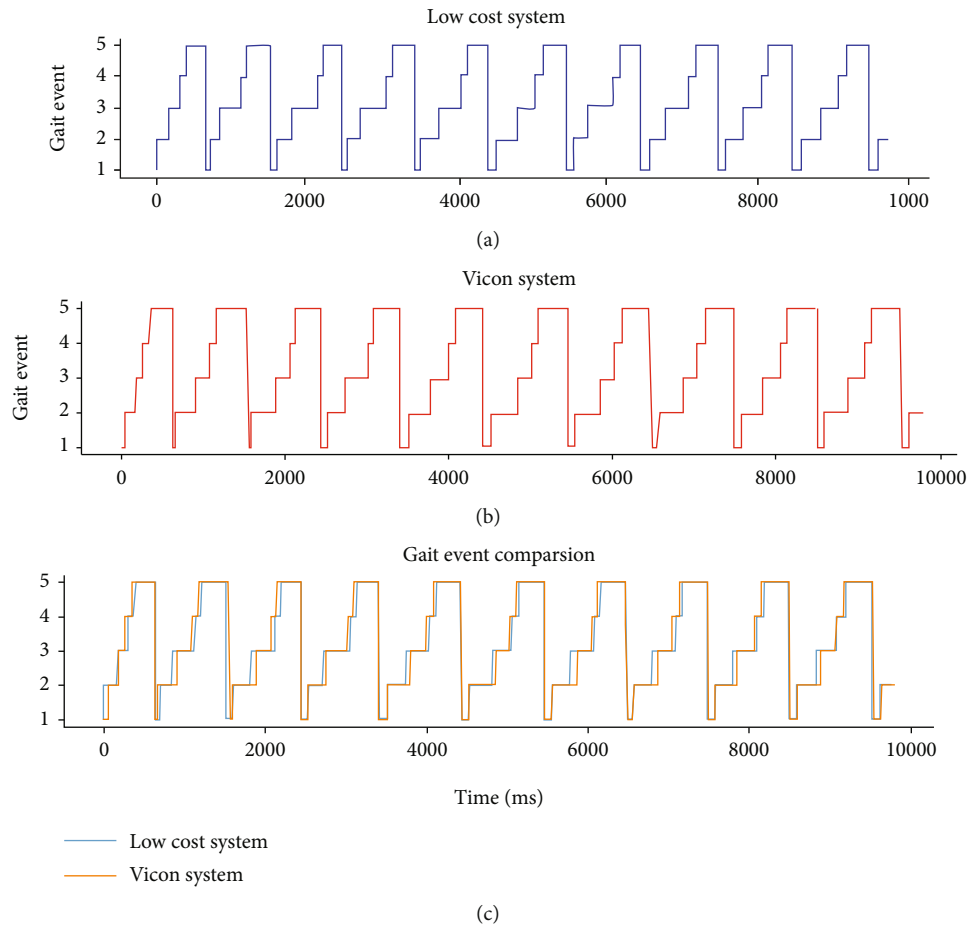


FIGURE 11: Gait event detection result comparison: (a) gait event detected by low-cost system; (b) gait event detected by Vicon system; (d) gait event comparison between two systems.

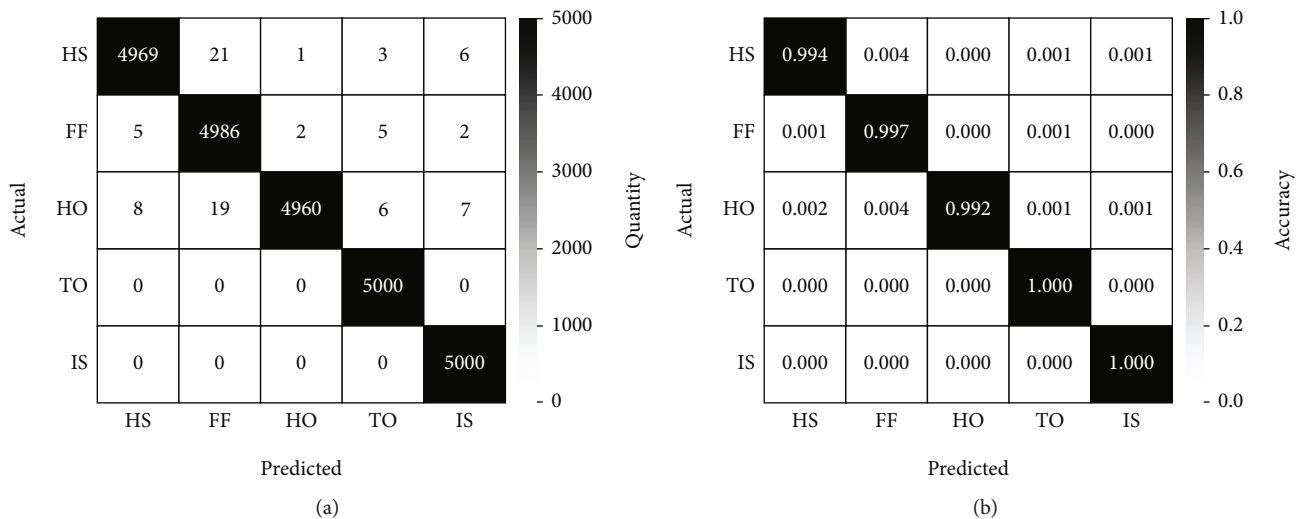


FIGURE 12: Confusion matrix of gait event detection result: (a) confusion matrix result; (b) normalized confusion matrix result.

The experiment obtains over 5000 gait samples, from 5 subjects, and the 5000 samples were adopted for accuracy calculation. Each subject was subjected to ground walking on the treadmill with a regular walking speed (4.2 km/h), and 1000 walking samples are recorded. A confusion matrix is adopted

to illustrate the detection accuracy of each gait event. Figure 12(a) shows the number of correct detections, whereas Figure 12(b) indicates the normalised detection accuracy. The result indicates that the LMIS achieves excellent performance on GED with an average of 99.66% accuracy.

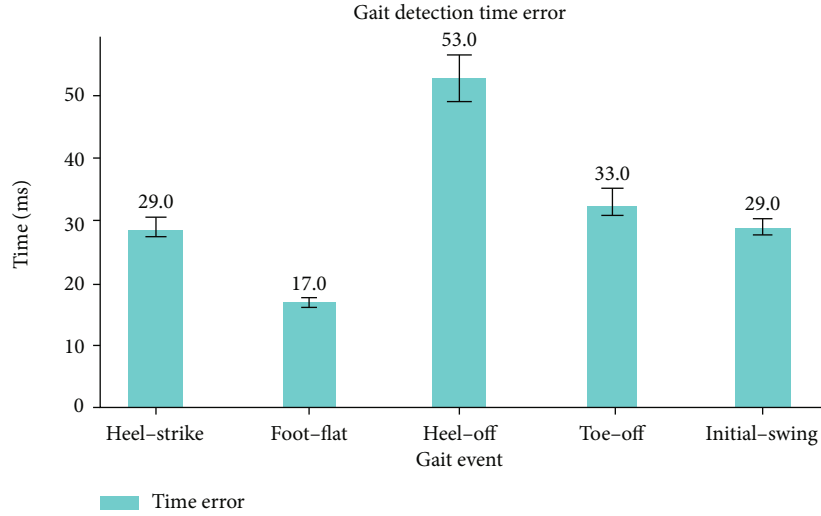


FIGURE 13: Gait detection time error.

TABLE 2: Gait event error types.

Error type	Definition
Critical error (e1)	Time error > 100 ms or wrong gait prediction
Noncritical error (e2)	Time error < 10 ms

Moreover, the confusion matrix also indicates that the LMIS has a stable performance for each single GED. For HS and FF, the accuracy of TO and SW event detection is 100 percent, 99.4%, and 99.7%, respectively. For HS and FF, the accuracy of TO and SW event detection is 100%, 99.4%, and 99.7%, respectively. Even in the worst-case scenario, the HO event detection accuracy remains 99.2%.

5.2. Time Error of the LMIS. The difference between the time reported by LMIS and the time reported by the referenced Vicon system at the same gait event is called the time error. LMIS achieved both high gait detection accuracy and low time error. For the five gait phases, 32 ms time errors appeared on average relative to the reference signal from the Vicon system.

According to the prediction result of the five gait events, the time error is 29 ms for HS, 17 ms for FF, 53 ms for HO, 33 ms for TO, and 29 ms for IS, as shown in Figure 13.

Since the Vicon system adopts a video signal and LMIS is a kind of kinematic-based measurement, the different measurement methods lead to the time error. Taking the HS event as an example, the video-based Vicon system can record the first time when the heel's marker touches the ground in coordination, whereas the ground reaction force is kinematically applied afterward which leads to a time gap. Similarly, during the HO event, the pressure was unloaded before the shoe goes off the ground, which has a time lag as well. Therefore, the detected gait event time by LMIS can either be earlier or later than the reference signal.

5.3. Accuracy Analysis regarding Time Error. Kostov [47] indicated that there are two kinds of errors in a machined learned rule in the gait event detector: "critical" and "noncritical" errors, where critical errors occur at the middle of the gait event and noncritical errors could shorten or extend each gait event. The critical errors lead to false GED and might result in the falling of users. Furthermore, the noncritical errors usually lead to time lag and do not influence the gait detection as much. In this study, the two types of errors are defined in Table 2.

Based on the two types of errors, two kinds of gait detection accuracies are adopted for gait detection performance evaluation: accuracy for e1 (A_{e1}) and accuracy for e2 (A_{e2}). A_{e1} is the relative difference of G_{e1} for the G_a , whereas A_{e2} equals the relative difference of G_{e2} for the G_a .

$$A_{e1} = \frac{G_a - G_{e1}}{G_a} \times 100\%, \quad (4)$$

$$A_{e2} = \frac{G_a - G_{e2}}{G_a} \times 100\%. \quad (5)$$

The A_{e1} of all five subjects during the gait experiment is 99.66% with 0.0073 standard deviations and A_{e2} is 76.26% with 0.1787 standard deviations. The detection accuracy result of each gait event is shown in Figure 14. Meanwhile, the detailed results of gait detection accuracy and standard deviation of each subject are shown (Appendix Table A4 and Table A5).

5.4. Performance Comparison with Other Projects. The LMIS presented in this study can reach an average of 99.66% accuracy for five different subjects regarding gait detection accuracy. This accurate detection rate is relatively higher than most of the existing gait detecting systems. The accuracy of traditional GPDS was 99%, as it only adopted a threshold-based filter to classify gait events. When compared with the project of Lee et al. [48], it reached a 99.15% detection rate when the peaks of foot acceleration identified gait events.

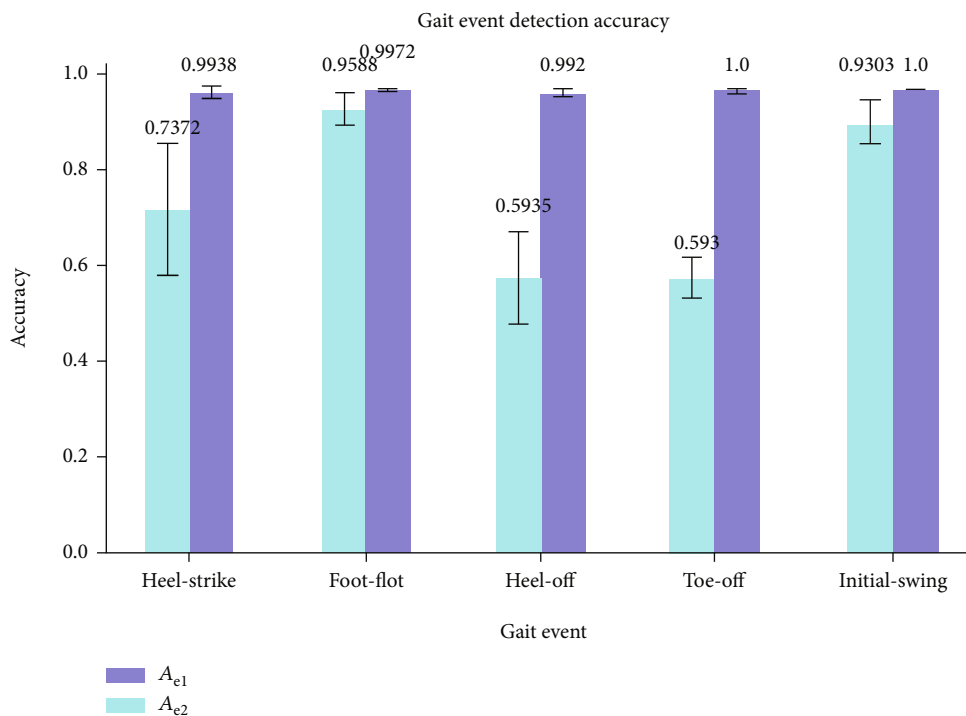


FIGURE 14: Gait detection accuracy.

The study of Rueterbories et al. [49] identifies the gait phase by differential foot acceleration with the gait detection accuracy of 99.66%. Although in the project of Kotiadis et al. [50], their system reached 100% gait detection accuracy, it was an offline method and had considerable time delay (0.03 Hz low-pass filter).

In terms of the gait detection time error, the average time error in LMIS is 32 ms which is relatively low compared to some existing researches. As per the time errors shown in Table 1, there appear 20 ms and 33 ms time errors for HS and toe-off stages in the proposed system. In contrast, these time errors are fewer than traditional GPDS [37] (90 ms for HS and 60 ms for TO) and Skelly and Chizeck [43] (120 ms for HS and 34 ms for TO). As GPDS and Skelly and Chizeck's project were pretty outdated, more recent works were required for comparison. However, the result in this study is still better than those in the studies of González [32] (117 ms for HS and 34 ms for TO) and Zhou [33] (average of 146.6 ms for HS and 70.4 ms for TO). When it comes to iIMU [44], the system presented outperforms the presented system which has lower time errors. Nevertheless, the iIMU can only start from FF conditions which means it does not work at the first gait cycle if the user is not in the stance status and it may result in falling. Also, it only adopts a 30 FPS video recording system (13 M pixels, 30 FPS) which itself has 33 ms errors per frame. Therefore, the actual time error could be much higher than expected. Furthermore, some projects do achieve fewer time errors compared to the presented projects. For example, the GPDS has a 40 ms time error in HO event which is smaller than our research (53 ms). Besides, Maqbool et al.'s research achieves lower time errors in all gait events (16 ms for HS, 16.5 ms for FF, 3.6 ms for HO, and 16 ms for

TO) [35]. It achieves a much lower time error in HO and TO events compared to most existing systems.

6. Conclusions

This article develops and validates an LMIS for online walking gait detection. The LMIS adopts mass-produced chips to achieve similar gait detection performance as the commercial Vicon system with lower prices. The high gait detection accuracy (99.66%), minor time error (32 ms), and low-cost (around 800£) characteristics indicated that the proposed system is a potential economic replacement for the Vicon system in the gait detection field.

The experiment validates the high reliability of the proposed system. The test results show 100% detection accuracy for TO and IS, 99.4% for HS, 99.7% for FF, and 99.2% for HO across all subjects in regular walking speed (4.2 km/h). It has a relatively low time error in FF (17 ms) and IS (29 ms) compared to other researches. However, this system indicates a higher time delay in HO (53 ms) and TO (33 ms). It indicates the algorithm should be improved to minimise the detection latency, especially in HO and TO events. Besides, the experiment is conducted under a specific walking speed, and varied speeds may influence the gait detection performance. The influence of different velocities should be analysed in a further experiment.

Data Availability

The gait detection result data used to support the findings of this study are included within the supplementary information file(s).

Conflicts of Interest

The authors declare no conflict of interest.

Acknowledgments

Authors would like to thank the University of Manchester and all the volunteers for their contributions.

Supplementary Materials

The appendix is attached within the supplement files and includes five tables. Table A1 shows the basic information of subjects. Tables A2 and A3 indicate the technical information of the LMIS and Vicon system, respectively. Tables A4 and A5 show the gait detection accuracy of each subject with respect to A_{e1} and A_{e2} . (*Supplementary Materials*)

References

- [1] D. Cowie, P. Limousin, A. Peters, and B. L. Day, "Insights into the neural control of locomotion from walking through doorways in Parkinson's disease," *Neuropsychologia*, vol. 48, no. 9, pp. 2750–2757, 2010.
- [2] A. Tanigawa, S. Morino, T. Aoyama, and M. Takahashi, "Gait analysis of pregnant patients with lumbopelvic pain using inertial sensor," *Gait & Posture*, vol. 65, pp. 176–181, 2018.
- [3] S. Qiu, Z. Wang, H. Zhao, K. Qin, Z. Li, and H. Hu, "Inertial/magnetic sensors based pedestrian dead reckoning by means of multi-sensor fusion," *Information Fusion*, vol. 39, pp. 108–119, 2018.
- [4] H. Zhao, Z. Wang, S. Qiu et al., "Heading drift reduction for foot-mounted inertial navigation system via multi-sensor fusion and dual-gait analysis," *IEEE Sensors Journal*, vol. 19, no. 19, pp. 8514–8521, 2019.
- [5] Z. Li, Z. Ren, K. Zhao, C. Deng, and Y. Feng, "Human-cooperative control design of a walking exoskeleton for body weight support," *IEEE Transactions on Industrial Informatics*, vol. 16, pp. 2985–2996, 2019.
- [6] Q. Wei, Z. Li, and K. Zhao, "Synergy-based control of assistive lower-limb exoskeletons by skill transfer," *IEEE/ASME Transactions on Mechatronics*, vol. 25, pp. 705–715, 2020.
- [7] S. Borel, P. Schneider, and C. Newman, "Video analysis software increases the interrater reliability of video gait assessments in children with cerebral palsy," *Gait & Posture*, vol. 33, no. 4, pp. 727–729, 2011.
- [8] W. Dickens and M. Smith, "Validation of a visual gait assessment scale for children with hemiplegic cerebral palsy," *Gait & Posture*, vol. 23, no. 1, pp. 78–82, 2006.
- [9] S. Liu, Q. Wang, and Y. Luo, "A review of applications of visual inspection technology based on image processing in the railway industry," *Transportation Safety and Environment*, vol. 1, no. 3, pp. 185–204, 2020.
- [10] E. Ott, M. Munih, H. Benko, and A. Kralj, "Comparison of foot-switch and hand switch triggered FES correction of foot drop," in *Proceedings of the 6th Vienna International Workshop on Functional Electrical Stimulation*, pp. 22–24, Vienna, 1998.
- [11] M. R. Popovic, T. Keller, I. P. I. Papas, V. Dietz, and M. Morari, "Surface-stimulation technology for grasping and walking neuroprostheses," *IEEE Engineering in Medicine and Biology Magazine*, vol. 20, no. 1, pp. 82–93, 2001.
- [12] D. Rongching, R. B. Stein, B. J. Andrews, K. B. James, and M. Wieler, "Application of tilt sensors in functional electrical stimulation," *IEEE Transactions on Rehabilitation Engineering*, vol. 4, no. 2, pp. 63–72, 1996.
- [13] D. van der Wilk, R. Reints, K. Postema et al., "Development of an ankle-foot orthosis that provides support for flaccid paretic plantarflexor and dorsiflexor muscles," *IEEE Transactions on Neural Systems and Rehabilitation Engineering*, vol. 26, no. 5, pp. 1036–1045, 2018.
- [14] S. K. Ng and H. J. Chizeck, "Fuzzy model identification for classification of gait events in paraplegics," *IEEE Transactions on Fuzzy Systems*, vol. 5, no. 4, pp. 536–544, 1997.
- [15] A. Kostov, B. J. Andrews, D. B. Popovic, R. B. Stein, and W. W. Armstrong, "Machine learning in control of functional electrical stimulation systems for locomotion," *IEEE Transactions on Biomedical Engineering*, vol. 42, no. 6, pp. 541–551, 1995.
- [16] B. Ugurlu, H. Oshima, E. Sariyildiz, T. Narikiyo, and J. Babic, "Active compliance control reduces upper body effort in exoskeleton-supported walking," *IEEE Transactions on Human-Machine Systems*, vol. 50, no. 2, pp. 144–153, 2020.
- [17] R. W. Jackson and S. H. Collins, "Heuristic-based ankle exoskeleton control for co-adaptive assistance of human locomotion," *IEEE Transactions on Neural Systems and Rehabilitation Engineering*, vol. 27, no. 10, pp. 2059–2069, 2019.
- [18] J. Zhang, P. Fiers, K. A. Witte et al., "Human-in-the-loop optimization of exoskeleton assistance during walking," *Science*, vol. 356, no. 6344, pp. 1280–1284, 2017.
- [19] W. Huo, S. Mohammed, and Y. Amirat, "Impedance reduction control of a knee joint human-exoskeleton system," *IEEE Transactions on Control Systems Technology*, vol. 27, no. 6, pp. 2541–2556, 2019.
- [20] T. Hussain, N. Iqbal, H. Maqbool, M. Khan, M. Awad, and A. Dehghani-Sanij, "Intent based recognition of walking and ramp activities for amputee using sEMG based lower limb prostheses," *Biocybernetics and Biomedical Engineering*, vol. 40, no. 3, pp. 1110–1123, 2020.
- [21] N. Hegde, M. Bries, and E. Sazonov, "A comparative review of footwear-based wearable systems," *Electronics*, vol. 5, no. 4, pp. 48–48, 2016.
- [22] Y. Guo and Lanmei, "Recent advance in plantar pressure measurement system," *Sensors Transducers*, vol. 145, pp. 96–105, 2012.
- [23] L. Carcreff, C. Gerber, A. Paraschiv-Ionescu et al., "What is the best configuration of wearable sensors to measure spatiotemporal gait parameters in children with cerebral palsy?," *Sensor*, vol. 18, no. 2, p. 394, 2018.
- [24] A. M. Sabatini, C. Martelloni, S. Scapellato, and F. Cavallo, "Assessment of walking features from foot inertial sensing," *IEEE Transactions on Biomedical Engineering*, vol. 52, no. 3, pp. 486–494, 2005.
- [25] C. Moufawad el Achkar, C. Lenoble-Hoskovec, A. Paraschiv-Ionescu, K. Major, C. Büla, and K. Aminian, "Physical behavior in older persons during daily life: insights from instrumented shoes," *Sensors*, vol. 16, no. 8, pp. 1225–1225, 2016.
- [26] J. C. M. Schlachetzki, J. Barth, F. Marxreiter et al., "Wearable sensors objectively measure gait parameters in Parkinson's disease," *PLoS One*, vol. 12, no. 10, p. e0183989, 2017.
- [27] L. Shu, T. Hua, Y. Wang, Q. Qiao Li, D. D. Feng, and X. Tao, "Inshoe plantar pressure measurement and analysis system

- based on fabric pressure sensing array," *IEEE Transactions on Information Technology in Biomedicine*, vol. 14, no. 3, pp. 767–775, 2010.
- [28] A. M. Tan, F. K. Fuss, Y. Weizman, Y. Woudstra, and O. Troynikov, "Design of low cost smart insole for real time measurement of plantar pressure," *Procedia Technology*, vol. 20, pp. 117–122, 2015.
- [29] W. Xu, Z. Li, M. C. Huang, N. Amini, and M. Sarrafzadeh, "An eTextile device for sitting posture monitoring," *Body Sensor Network*, vol. 1, pp. 194–199, 2011.
- [30] C. A. Macleod, B. A. Conway, D. B. Allan, and S. S. Galen, "Development and validation of a low-cost, portable and wireless gait assessment tool," *Medical Engineering & Physics*, vol. 36, no. 4, pp. 541–546, 2014.
- [31] B. Horsak, R. Dlapka, M. Iber et al., "SONIGait: a wireless instrumented insole device for real-time sonification of gait," *Journal on Multimodal User Interfaces*, vol. 10, no. 3, pp. 195–206, 2016.
- [32] R. C. González, A. M. López, J. Rodríguez-Uría, D. Álvarez, and J. C. Alvarez, "Real-time gait event detection for normal subjects from lower trunk accelerations," *Gait & Posture*, vol. 31, no. 3, pp. 322–325, 2010.
- [33] H. Zhou, "Towards real-time detection of gait events on different terrains using time-frequency analysis and peak heuristics algorithm," *Sensors*, vol. 16, no. 10, pp. 1634–1634, 2016.
- [34] N. Chia Bejarano, E. Ambrosini, A. Pedrocchi, G. Ferrigno, M. Monticone, and S. Ferrante, "A novel adaptive, real-time algorithm to detect gait events from wearable sensors," *IEEE Transactions on Neural Systems and Rehabilitation Engineering*, vol. 23, no. 3, pp. 413–422, 2015.
- [35] H. Maqbool, M. Husman, M. Awad et al., "Heuristic real-time detection of temporal gait events for lower limb amputees," *IEEE Sensors Journal*, vol. 19, no. 8, pp. 3138–3148, 2019.
- [36] M. Goršič, R. Kamnik, L. Ambrožič et al., "Online phase detection using wearable sensors for walking with a robotic prosthesis," *Sensors*, vol. 14, no. 2, pp. 2776–2794, 2014.
- [37] I. P. I. Pappas, M. R. Popovic, T. Keller, V. Dietz, and M. Morari, "A reliable gait phase detection system," *IEEE Transactions on Neural Systems and Rehabilitation Engineering*, vol. 9, no. 2, pp. 113–125, 2001.
- [38] S. Mazilu, M. Hardegger, Z. Zhu et al., "Online detection of freezing of gait with smartphones and machine learning techniques," in *6th International Conference on PervasiveHealth and Workshops*, pp. 123–130, San Diego, California, United States, 2012.
- [39] S. J. Preece, J. Y. Goulermas, L. P. J. Kenney, D. Howard, K. Meijer, and R. Crompton, "Activity identification using body-mounted sensors—a review of classification techniques," *Physiological Measurement*, vol. 30, no. 4, pp. R1–R33, 2009.
- [40] H. Lakany, "Extracting a diagnostic gait signature," *Pattern Recognition*, vol. 41, no. 5, pp. 1627–1637, 2008.
- [41] R. K. Begg, M. Palaniswami, and B. Owen, "Support vector machines for automated gait classification," *IEEE Transactions on Biomedical Engineering*, vol. 52, no. 5, pp. 828–838, 2005.
- [42] B. Pogorelc, Z. Bosnić, and M. Gams, "Automatic recognition of gait-related health problems in the elderly using machine learning," *Multimedia Tools and Applications*, vol. 58, no. 2, pp. 333–354, 2012.
- [43] M. M. Skelly and H. J. Chizeck, "Real-time gait event detection for paraplegic FES walking," *IEEE Transactions on Neural Systems and Rehabilitation Engineering*, vol. 9, no. 1, pp. 59–68, 2001.
- [44] S. Ding, X. Ouyang, T. Liu, Z. Li, and H. Yang, "Gait event detection of a lower extremity exoskeleton robot by an intelligent IMU," *IEEE Sensors Journal*, vol. 18, no. 23, pp. 9728–9735, 2018.
- [45] A. Sabatini, "Kalman-filter-based orientation determination using inertial/magnetic sensors: observability analysis and performance evaluation," *Sensors*, vol. 11, no. 10, pp. 9182–9206, 2011.
- [46] A. Anwary, H. Yu, and M. Vassallo, "Optimal foot location for placing wearable IMU sensors and automatic feature extraction for gait analysis," *IEEE Sensors Journal*, vol. 18, no. 6, pp. 2555–2567, 2018.
- [47] A. Kostov, "Functional error assessment in gait event discrimination for FES assisted locomotion," in *Proceedings of 18th Annual International Conference of the IEEE Engineering in Medicine and Biology Society*, pp. 969–969, Amsterdam, Netherlands, 1996.
- [48] J. A. Lee, S. H. Cho, Y. J. Lee, H. K. Yang, and J. W. Lee, "Portable activity monitoring system for temporal parameters of gait cycles," *Journal of Medical Systems*, vol. 34, no. 5, pp. 959–966, 2010.
- [49] J. Rueterbories, E. G. Spaich, and O. K. Andersen, "Gait event detection for use in FES rehabilitation by radial and tangential foot accelerations," *Medical Engineering & Physics*, vol. 36, no. 4, pp. 502–508, 2014.
- [50] D. Kotiadis, H. J. Hermens, and P. H. Veltink, "Inertial gait phase detection for control of a drop foot stimulator: inertial sensing for gait phase detection," *Medical Engineering & Physics*, vol. 32, no. 4, pp. 287–297, 2010.